

Multiparameter elastic FWI for joint inversion of velocity and reflectivity

G. Huang¹, C. Macesanu¹, F. Liu¹, J. Ramos-Martinez¹, D. Whitmore¹, C. Calderon¹, R. Bloor¹

¹ TGS

Summary

We propose a multiparameter elastic FWI to simultaneously invert P-wave velocity and reflectivity. Our theoretical framework consists of two main elements for achieving this multiparameter inversion. First, we reformulate the system of waves equations parameterized in terms of P- and S-wave velocities as well as vector reflectivity. Second, we derive the sensitivity kernels for P-wave velocity and vector reflectivity using inverse scattering theory, which effectively reduce the crosstalk between parameters. We apply the algorithm to a dataset acquired in a complex salt environment in offshore Brazil. The results demonstrate the advantages of extending the multiparameter inversion approach to the elastic case compared to the acoustic version.

Multiparameter elastic FWI for joint inversion of velocity and reflectivity

Introduction

Full waveform inversion (FWI) has the potential for providing attributes besides velocity, that can assist in the detection and characterization of economic reservoirs. There has been an increasing interest in determining reflectivity from FWI algorithms (Wang et al., 2020). The main concept is to derive the pseudo-reflectivity from a high-frequency velocity model out of reflection FWI. This is a powerful approach for simplifying the seismic processing workflow and obtaining high resolution images. In this context, Yang et al. (2021) introduced an acoustic multiparameter FWI approach for simultaneously inverting velocity and reflectivity, through the mitigation of crosstalk between the two parameters. This approach makes plausible the implicit computation of the relative impedance from the reflectivity and velocity fields (Pankov, et al., 2023). This information can help in deriving valuable attributes used for quantitative interpretation, which require good amplitude fidelity.

The multiparameter FWI approach introduced by Yang et al. (2021) comprises two fundamental elements: a parameterization of the wave-equation in terms of velocity and reflectivity (Whitmore et al., 2020), and a robust algorithm that performs scale separation of the wavenumber components in the FWI gradient (Ramos-Martinez et al., 2016). The resulting wave equation is a proxy of the acoustic wave equation with variable density. The scale separation minimizes the crosstalk between velocity and reflectivity in the multiparameter inversion: low and intermediate wavenumbers determine the background velocity, whereas the high wavenumber contents invert the reflectivity. For geological settings with small impedance contrasts, these provide insightful information to identify cases in which the background velocity and impedance change might not directly correlate to one another (Korsmo, et al, 2024). In geologically complex areas with presence of high velocity contrasts, such as geobodies (e.g., salt and/or carbonates), it is essential to incorporate more comprehensive physics, like that found in an elastic algorithm (e.g. Liu, et al., 2024).

Here we introduce elastic multiparameter inversion for simultaneously inverting P-wave velocity and P-reflectivity. We derived a new elastic wave equation parameterized in terms of velocity and reflectivity. We present sensitivity kernels for P-wave velocity and reflectivity based on the adjoint-state method and discuss the scale separation for FWI gradient. We illustrate the method using a field OBN data set from offshore Brazil with a complex overburden over a presalt geology target.

Theory

Below we describe the elastic wave equations for joint inversion of P-wave velocity and P-wave reflectivity in a 3D elastic media. Similar to the acoustic case described in Whitmore et al. (2020), the employed system of elastic wave equations are as follows,

$$\frac{\partial \tilde{v}_i}{\partial t} = \frac{\partial \sigma_{ij}}{\partial x_j} \quad (1)$$

$$\frac{\partial \sigma_{ij}}{\partial t} = \tilde{c}_{ijkl} \frac{\partial \tilde{v}_k}{\partial x_l} - \tilde{c}_{ijkl} \left(2r_l^p - \frac{1}{V_p} \frac{\partial V_p}{\partial x_l} \right) \tilde{v}_k \quad (2)$$

where \tilde{v}_i is the weighted particle velocity wavefield (v_i) along the three spatial directions, which are functions of space \mathbf{x} and time t ; σ_{ij} represent the stress tensor with six independent dynamic fields, \tilde{c}_{ijkl} is the weighted stiffness tensor c_{ijkl} , which depends only on velocities and Thompsons parameters, V_p is the P-wave velocity and r_l^p is the P-wave vector reflectivity. A similar form of the equations can be found in Macesanu et al. (2024).

The corresponding sensitivity kernel for the P-wave velocity can be expressed as,

$$J_{V_p}(\mathbf{x}) = \int \left(W_1 \frac{1}{V_p^2} \frac{\partial \sigma_{jj}(\mathbf{x}, t)}{\partial t} \frac{\partial \widehat{\tau}_{ii}(\mathbf{x}, T-t)}{\partial t} + W_2 \frac{\partial \sigma_{jj}(\mathbf{x}, t)}{\partial x_k} \frac{\partial \widehat{\tau}_{ii}(\mathbf{x}, T-t)}{\partial x_k} \right) dt \quad (3)$$

and the one for the P wave vector reflectivity r_k^p is

$$J_{r_k^p}(\mathbf{x}) = \frac{\partial (J_{Z_p}(\mathbf{x}))}{\partial x_k} \quad (4)$$

$$J_{Z_p}(\mathbf{x}) = \int \left(W_3 \frac{1}{V_p^2} \frac{\partial \sigma_{jj}(\mathbf{x}, t)}{\partial t} \frac{\partial \widehat{\tau}_{ii}(\mathbf{x}, T-t)}{\partial t} - W_4 \frac{\partial \sigma_{jj}(\mathbf{x}, t)}{\partial x_k} \frac{\partial \widehat{\tau}_{ii}(\mathbf{x}, t)}{\partial x_k} \right) dt \quad (5)$$

where $\widehat{\tau}_{ii}$ are the back-propagated tensor fields with the data residuals as source, and the coefficients W_1, W_2, W_3, W_4 are the dynamic weights for optimal scale separation.

Figure 1 shows impulse responses computed from equations (3) and (5) for a single source-receiver pair in a homogeneous elastic layer overlying an elastic half-space. Different scales are cleanly separated and used to invert the P-wave velocity and reflectivity.



Figure 1 Sensitivity kernels of a source-receiver pair for a homogeneous layer overlying a half-space: (a) conventional P-wave velocity kernel, (b) P-wave reflectivity kernel and (c) P-wave velocity kernel.

Field data Example

We apply the new algorithm to OBN data acquired in deep water Santos Basin, offshore Brazil. This dataset consists of 954 stations covering an area of approximately 111 km² with sources covering about 345 km². In this deep-water setting, there are significant imaging challenges imposed by a complex overburden with large impedance contrasts complicating imaging the pre-salt region (Burren, et al., 2025). The inversion was performed in the bandwidth of 2 Hz to 25 Hz using data with minimal pre-processing consisting mainly of debubble and noise attenuation.

In Figure 2, we compare one inline and one crossline sections, with panels (a) and (c) showing the inverted velocity models from the multiparameter acoustic inversion, and panels (b) and (d) displaying the same lines from the elastic implementation. The acoustic algorithm produces a less focused boundary at the top of the salt with spurious variations in velocity at the interface. Consequently, the inverted reflectivity exhibits a less defined salt boundary (Figures 2e and 2g). In contrast, the elastic algorithm, which incorporates more physics, produces a much more focused boundary with a higher resolution at the top of the salt (Figures 2b and 2d). The correspondingly inverted reflectivity also shows enhanced resolution for the salt boundary (Figures 2f and 2h). Compared to the acoustic reflectivity (Figures 2e and 2g), the elastic inversion (Figures 2f and 2h) shows higher resolution and better reflector continuity. This is more evident in the better-resolved fault structures in both postsalt and presalt sequences. In Figure 3, we compare a depth slice of the two inverted reflectivity models, with the elastic result in Figure 3b clearly showing a more focused image and improved resolution at salt boundary.

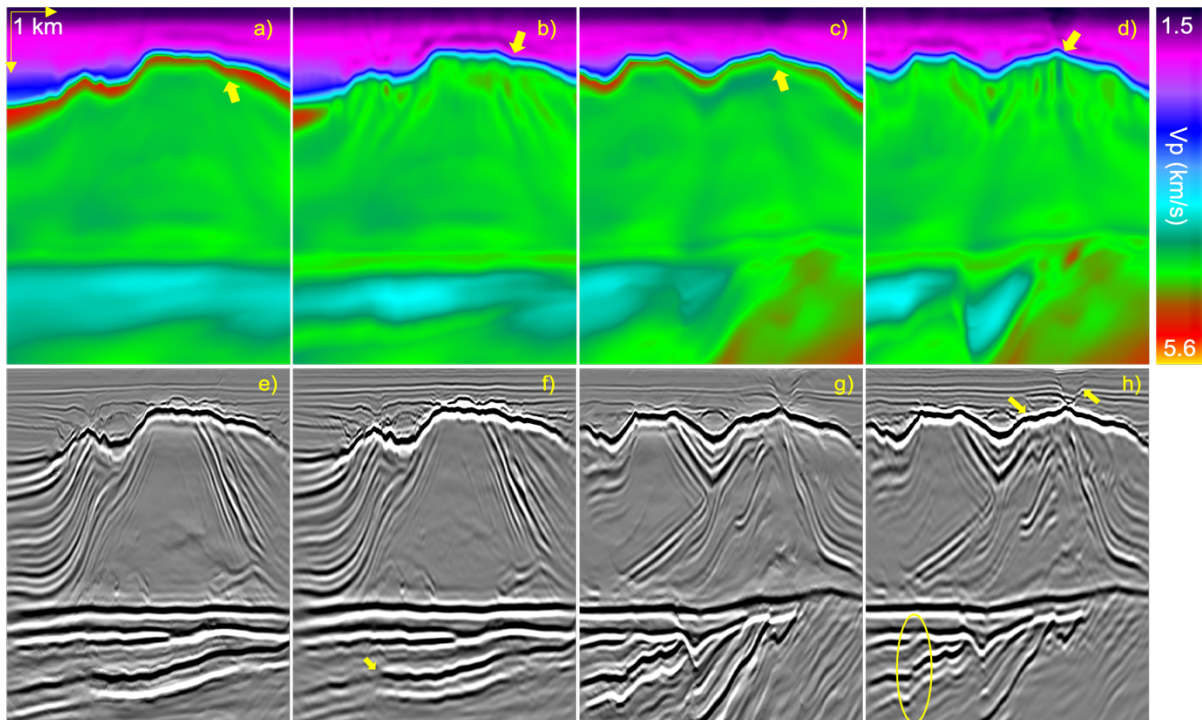


Figure 2. Comparison of the inverted P-wave velocity and normal reflectivity: (a) and (c) are one inline and one crossline of acoustic inverted velocity; (e) and (g) are the corresponding reflectivity; (b) and (d) are the velocity from the elastic inversion and (f) and (h) are their corresponding reflectivity.

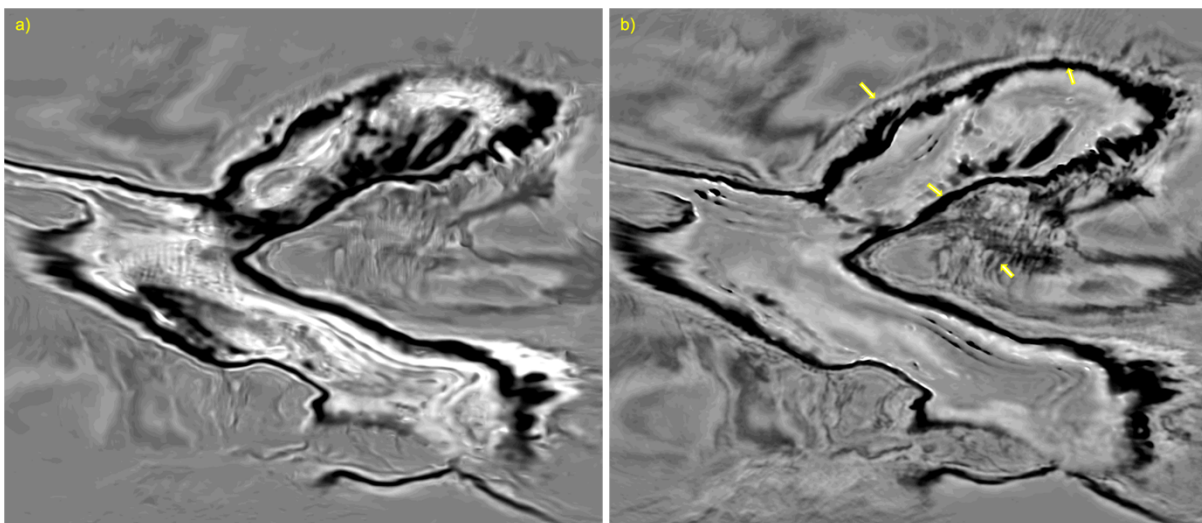


Figure 3. One depth slice of the inverted normal reflectivity using (a) acoustic and (b) elastic algorithm. The yellow arrows point to enhanced imaging with better continuity and more focused salt boundary.

Conclusions

We introduce a multiparameter elastic FWI algorithm that estimates P-wave velocity and P-wave reflectivity for elastic media. Our implementation facilitates the construction of the necessary parameters for the elastic inversion. In addition, it reduces the cross-talk between the inverted parameters. Results from field data demonstrate the advantages of the multiparameter elastic inversion compared to the acoustic case. This framework can be extended to the mode converted waves (PS) and the corresponding reflectivity inversion, which is of particular interest for reservoir characterization.

Acknowledgements

We acknowledge TGS for granting us authorization to publish this material. We thank Petrobras for providing access to their dataset. We appreciate the insightful discussions with Eric Frugier and Mariana Gherasim.

References

Burren, J., Frugier, E. and Korsmo, Ø. [2025] Multiparameter inversion of velocity and reflectivity applied to ocean bottom node data from offshore Brazil. *86th EAGE Conference & Exhibition*, Extended Abstracts.

Korsmo, Ø., Pankov, A., Caselitz, B., Kumar, J. [2024] Reservoir focused imaging with simultaneous inversion of velocity and angle dependent reflectivity. *First EAGE Data Processing Workshop*, Cairo, Egypt.

Liu, F., Macesanu, C., Hu, H., Gao, F., Zhan, G., Huang Y., Sheng J., He, Y., Calderon, C. and Wang, B. [2024] Enhance P wave imaging using elastic dynamic matching FWI. *85th EAGE Conference & Exhibition*, Extended Abstracts.

Macesanu, C., Liu, F., Huang, Y., Mao, H. and Calderon, C. [2024] Implementation aspects of elastic FWI and its application to sparse OBN data. *Fourth International Meeting for Applied Geoscience and Energy, Expanded Abstracts*, 886-890.

Pankov, A., Ackers, M., Korsmo, Ø., Reiser, C., Rønholt, G., Cock, C.H. and Tjensvoll, V. [2023] Application of simultaneous inversion (FWI and nonlinear LS-RTM) for improved imaging. *84th EAGE Conference & Exhibition*, Extended Abstracts.

Ramos-Martinez, J., Crawley, S., Zou, K., Valenciano, A.A., Qiu, L. and Chemingui, N. [2016] A robust gradient for long wavelength FWI updates, *78th EAGE Conference & Exhibition*, Extended Abstracts.

Whitmore, N.D., Ramos-Martinez, J., Yang, Y. and Valenciano, A.A. [2020] Full wave field modelling with vector-reflectivity, *82nd EAGE Conference & Exhibition*, Extended Abstracts.

Yang, Y., Ramos-Martinez, J., Whitmore, D., Guanghui, H. and Chemingui, N. [2021] Simultaneous inversion of velocity and reflectivity. *First Break*, **39**(12), 55-59.

Wang, B., He, Y., Mao, J., Liu, F., Hao, F., Perz, M. and Mitchel, S. [2021] Inversion-based imaging: LSRTM to FWI Imaging. *First Break*, **39**(12), 85-93.